Commun. Comput. Phys.
doi: 10.4208/cicp.160914.270315a

Vol. **19**, No. 1, pp. 94-123
January 2016

ADI-FDTD Method for Two-Dimensional Transient Electromagnetic Problems

Wanshan Li[1], Yile Zhang[2,*], Yau Shu Wong[2] and Dong Liang[3]

[1] *School of Mathematics, Shandong University, Jinan 250199, P.R. China.*
[2] *Department of Mathematical and Statistical Sciences, University of Alberta, Edmonton, AB, T6G 2G1, Canada.*
[3] *Department of Mathematics and Statistics, York University, Toronto, ON, M3J 1P3, Canada.*

Received 16 September 2014; Accepted (in revised version) 27 March 2015

Abstract. An efficient and accurate numerical scheme is proposed for solving the transverse electric (TE) mode electromagnetic (EM) propagation problem in two-dimensional earth. The scheme is based on the alternating direction finite-difference time-domain (ADI-FDTD) method. Unlike the conventional upward continuation approach for the earth-air interface, an integral formulation for the interface boundary is developed and it is effectively incorporated to the ADI solver. Stability and convergence analysis together with an error estimate are presented. Numerical simulations are carried out to validate the proposed method, and the advantage of the present method over the popular Du-Fort-Frankel scheme is clearly demonstrated. Examples of the electromagnetic field propagation in the ground with anomaly further verify the effectiveness of the proposed scheme.

AMS subject classifications: 65N06, 65N12, 65N15, 65N22

Key words: ADI-FDTD, interface boundary, stability and convergence analysis.

1 Introduction

Interpretation of electromagnetic data in complex geological environments depends on the multidimensional forward and inverse modeling, and the topic is of great interest to geophysics community. The finite-difference time-domain (FDTD) method first introduced by Yee [44] and Taflove [38] is now generally regarded as one of the most commonly used tools in the EM exploration applications. Oristaglio and Hohmann [28] used the DuFort-Frankel scheme to simulate 2D transient response to the shut-off of a line

*Corresponding author. *Email addresses:* wanshanli@mail.sdu.edu.cn (W. Li), yile2@ualberta.ca (Y. Zhang), yauwong@ualberta.ca (Y. S. Wong), dliang@mathstat.yorku.ca (D. Liang)

source. Lepin [24] extended the FDTD scheme into 3D cases by using the Fourier transform along the strike direction, in which a 2D problem was solved for discrete wavenumbers. Such model is usually referred as a 2.5D problem, and it performs well for a general 3D structures [36]. Wang and Hohmann [42] extended the FDTD scheme to 3D applications, where the DuFort-Frankel scheme was employed with a staggered-grid. The divergence condition of the magnetic field was imposed and a displacement current term was introduced to ensure the numerical stability. Commer and Newman [4] developed a parallel version for 3D applications. By transforming the Maxwell equation to another form which was less frequency dependent, Maao achieved an efficient implementation of FDTD computation [25]. Other works basing on the finite difference including the hybrid finite-difference method and parallel computing were reported in [45] and [34].

In addition to the finite difference (FD) method, the finite volume (FV) and finite element (FE) methods have also been frequently used. The work on FV method covers both the frequency domain [5, 14] and time domain [15]. With the advantage of dealing well with complex geometric domains as well as complicated geologic interfaces, the FE method is very popular in time domain [16, 17] and in frequency domain [18]. Goldman et al. [10] applied the FE method in the spatial formulation for the 2D problem and the backward Euler method in the time-domain. Everett and Edwards [7] developed the finite-element time-domain (FETD) method to simulate the marine electromagnetic propagation in 2.5D case. Um et al. [41] developed an iterative FETD to investigate the diffusion behavior in 3D earth, where an adaptive time step doubling method was considered to reduce the computing time. Besides the time domain approaches, many work has also been reported in the frequency domain. Without the consideration of time step, it is particularly suitable for applying FE to 2D [23], 2.5D [20] and 3D [30, 40] problems. Recent development on the FE method in EM includes the edge-based FE method [3, 26], multifrontal method [6], adaptive FE method [12, 31], parallel computation [21, 30] and other inversion related problems [11, 32].

However, it is well known that the computing cost associated with FE method is very expensive. It is not a trivial task to generate a proper grid system, the more complex the earth structure is, the more cost there will be needed. Besides, since the resultant matrix in the FE method is frequently ill-conditioned, the solutions may require the use of direct methods [40, 41]. It is worth to note that the computational cost for a direct solver is $\mathcal{O}(N^3)$, therefore a tremendous amount of storage requirement and computing time are demanded.

Compared with the FETD approach, one attractive advantage of the FDTD algorithm lies in its straightforward implementation. It is feasible to implement an efficient FDTD code with limited computing and storage resource. Further improvements are possible by considering implicit FDTD because of their favorable stability condition as well as computing efficiency, such as ADI-FDTD, Symplectic-FDTD, EC-S-FDTD, etc [2, 5, 8, 9, 27, 37]. With its unconditional stability, the ADI method first introduced by Peaceman Rachford [29] and Douglas [19] could take larger time step than the explicit schemes. Moreover, it is easy to extend an ADI algorithm from 2D problems to 3D problems.

The storage requirement and computing cost usually depend on the model and the governing equations. Various FDTD formulations have been proposed using diffusion equation [4, 28, 42], Maxwell equations [22, 33, 43] and Helmholtz equation [35, 40, 41]. In this study, we consider a 2D model based on the diffusion equation simulating the electric field. The primary advantage of this choice is that the number of unknowns is much smaller than in other cases. The study of a 2D wave propagation problem is essential, since developing an efficient and accurate solution for a 2.5D model directly depends on the quality of the 2D scheme. Moreover, when implementing a 3D computational code, the 2D scheme can also be extended by adding variables without changing the governing equations.

The major contribution of the presented study are threefold. First, we implement accurate boundary conditions for the earth-air interface and the underground interface. A popular approach to avoid the discretization in the air is to extend one layer into the air [1, 4, 28, 42], and this procedure is known as upward continuation. Here, an integral equation is imposed at the earth-air interface, which provides an accurate relationship between the normal derivative and horizontal derivative of the electric field. The challenge is how to incorporate the integral equation numerically. Moreover, for the boundary in the earth, the Neumann boundary condition is applied instead of the PEC (i.e. Dirichlet type boundary condition) in order to reduce the reflection error. Secondly we propose the ADI-FDTD scheme including the treatment of a nonlocal boundary condition, which appears due to the integral boundary condition at the earth-air interface. The stability analysis and convergence order are reported. Finally, as an implicit scheme, numerical example demonstrates that the combined ADI-FDTD algorithm has a competitive advantage over the explicit FDTD in both efficiency and accuracy. This is because the ADI-FDTD is unconditionally stable and allows the use of larger time steps.

Our paper is organized as follows. In Section 2, we present the mathematical model for the 2D TEM problem with the boundary conditions in the earth-air interface and underground interface. The ADI-FDTD formulation for this model are reported in Section 3. Then, Sections 4 and 5 give the stability analysis and error estimate. The proposed ADI-FDTD scheme is validated, and numerical simulations are reported in Section 6.

2 TEM model

Consider a 2D transient electromagnetic (TEM) model in the x-z plane with a rectangular domain $\Omega=[0,a]\times[0,b]$ as depicted in Fig. 1, and the time interval is $[0,T]$. Under the quasi-stationary assumption of the Maxwell's equations, the TEM model is constructed as the following initial-boundary value (IBV) problem [28]:

$$\mu_0\sigma\frac{\partial E}{\partial t}-\frac{\partial^2 E}{\partial x^2}+\frac{\partial^2 E}{\partial z^2}=-\mu_0\frac{\partial J_s}{\partial t},\quad \text{in } \Omega, \tag{2.1}$$

$$\frac{\partial E}{\partial n}(x,z=b,t)+\frac{1}{\pi}P\int_{-\infty}^{+\infty}\frac{1}{x-x'}\frac{\partial E}{\partial x'}(x',z=b,t)dx'=0,\quad \text{on } \Gamma_1, \tag{2.2}$$

$$\frac{\partial E}{\partial n}=0,\quad \text{on } \Gamma_2,\Gamma_3,\Gamma_4, \tag{2.3}$$

where E is the electric field, μ_0 is the permeability of the free space, $\sigma=\sigma(x,z)$ is the conductivity distribution, J_s is the density of the source current in the y-direction. P represents a principal value integral and n is the outward pointing normal direction.

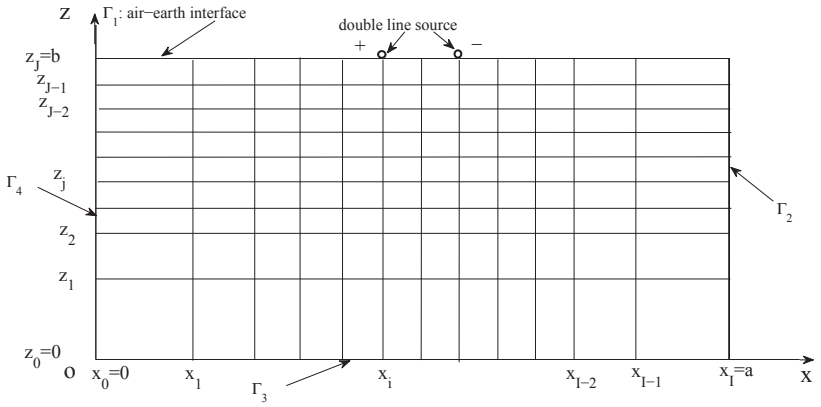

Figure 1: Geometry for the 2D TEM problem with the double line source.

The system (2.1)-(2.3) describes the electric field induced by the variation of the source J_s in the earth. Since the conductivity σ in the earth is normally much larger than the permittivity ϵ so that the wavelike features of the electric field vanish very quickly, therefore we consider the diffusion equation (2.1) as the governing equation. The upper boundary condition (2.2) is derived from the radiation boundary condition, it indicates the relationship to be satisfied for the electric field at the earth-air interface.

For the treatment of the earth-air interface in a 2D TEM modelling, a popular approach is to use the upward continuation by extending one layer into the air [28, 42]. Moreover, to avoid the reflection error from the Dirichlet boundary condition, the computation domain must be large enough so that the values at the subsurface boundaries to be the analytical solution for half-space.

In the present study, we handle the earth-air interface by imposing the exact integral boundary condition (2.2). In addition, the Dirichlet condition is replaced by a Neumann condition for the boundary in the earth (Γ_2, Γ_3, Γ_4) (2.3). For the simulation of a sufficiently large domain, this would significantly reduce the reflections from the subsurfaces.

In fact, to avoid the singularity at the early time, the excitation of EM responses from the shut-off of the current source J_s is generally replaced by imposing the initial conditions on the electric field. Thus, we set J_s to zero and adding the following initial condition:

$$E(x,z,0)=E_0(x,z),\quad \text{in } \Omega. \tag{2.4}$$

3 Numerical formulation for ADI-FDTD with integral boundary

In this section, the ADI-FDTD scheme is proposed for the IBV problem (2.1)-(2.4).

First, let us introduce the partition of the computation domain as displayed in Fig. 1, where x_i, $i=0,1,\cdots,I$, and z_j, $j=0,1,\cdots,J$, represent the mesh grids along the x and z directions, respectively. Here, z_J is the earth-air interface. Let t^n denote the discretization for the time interval $[0,T]$ and $\Delta t_n=t^n-t^{n-1}$ be the time step. Also define $x_{i+\frac{1}{2}}=(x_i+x_{i+1})/2$, $z_{j+\frac{1}{2}}=(z_j+z_{j+1})/2$ and $t^{n+\frac{1}{2}}=(t^n+t^{n+1})/2$. Let $\Delta x_i=x_i-x_{i-1}$, $\Delta z_j=z_j-z_{j-1}$ be the spatial steps in the x and z directions. Define the central-differential operators as:

$$\delta_x E_{i,j}=\frac{E_{i+\frac{1}{2},j}-E_{i-\frac{1}{2},j}}{x_{i+\frac{1}{2}}-x_{i-\frac{1}{2}}},\quad \delta_z E_{i,j}=\frac{E_{i,j+\frac{1}{2}}-E_{i,j-\frac{1}{2}}}{z_{j+\frac{1}{2}}-z_{j-\frac{1}{2}}},\tag{3.1}$$

where $x_{i+\frac{1}{2}}-x_{i-\frac{1}{2}}=\frac{1}{2}(\Delta x_i+\Delta x_{i+1})$, and $z_{j+\frac{1}{2}}-z_{j-\frac{1}{2}}=\frac{1}{2}(\Delta z_j+\Delta z_{j+1})$.

The proposed ADI-FDTD scheme for the TEM model (2.1)-(2.4) is constructed as follows:

Step 1: Compute the intermediate variable $E^{n+\frac{1}{2}}$ using E^n implicitly in the x direction and explicitly in the z direction.

$$\begin{aligned}&\mu\sigma_{i,j}\frac{E_{i,j}^{n+\frac{1}{2}}-E_{i,j}^n}{\Delta t_{n+1}/2}=\delta_x^2E_{i,j}^{n+\frac{1}{2}}+\delta_z^2E_{i,j}^n\\&=\frac{2(E_{i+1,j}^{n+\frac{1}{2}}-E_{i,j}^{n+\frac{1}{2}})}{\Delta x_{i+1}(\Delta x_i+\Delta x_{i+1})}-\frac{2(E_{i,j}^{n+\frac{1}{2}}-E_{i-1,j}^{n+\frac{1}{2}})}{\Delta x_i(\Delta x_i+\Delta x_{i+1})}\\&\quad+\frac{2(E_{i,j+1}^n-E_{i,j}^n)}{\Delta z_{j+1}(\Delta z_j+\Delta z_{j+1})}-\frac{2(E_{i,j}^n-E_{i,j-1}^n)}{\Delta z_j(\Delta z_j+\Delta z_{j+1})},\quad i=1,\cdots,I-1,\quad j=1,\ldots,J-1,\end{aligned}\tag{3.2}$$

with the following boundary conditions for Γ_2, Γ_3 and Γ_4:

$$E_{i,0}^{n+\frac{1}{2}}=E_{i,1}^{n+\frac{1}{2}},\quad E_{0,j}^{n+\frac{1}{2}}=E_{1,j}^{n+\frac{1}{2}},\quad E_{I,j}^{n+\frac{1}{2}}=E_{I-1,j}^{n+\frac{1}{2}}.\tag{3.3}$$

It is necessary to note that in the first step, there is no need to compute the values of the intermediate variable $E^{n+\frac{1}{2}}$ on the upper boundary Γ_1 since they would not be used in the second-step calculation.

To clarify the computing procedure of this step, the scheme (3.2) is rearranged as:

$$\begin{aligned}&\left(1+\frac{\Delta t_{n+1}}{\mu\sigma_{i,j}\Delta x_i(\Delta x_i+\Delta x_{i+1})}+\frac{\Delta t_{n+1}}{\mu\sigma_{i,j}\Delta x_{i+1}(\Delta x_i+\Delta x_{i+1})}\right)E_{i,j}^{n+\frac{1}{2}}\\&\quad-\frac{\Delta t_{n+1}}{\mu\sigma_{i,j}\Delta x_i(\Delta x_i+\Delta x_{i+1})}E_{i-1,j}^{n+\frac{1}{2}}-\frac{\Delta t_{n+1}}{\mu\sigma_{i,j}\Delta x_{i+1}(\Delta x_i+\Delta x_{i+1})}E_{i+1,j}^{n+\frac{1}{2}}\\=&\left(1-\frac{\Delta t_{n+1}}{\mu\sigma_{i,j}\Delta z_j(\Delta z_j+\Delta z_{j+1})}-\frac{\Delta t_{n+1}}{\mu\sigma_{i,j}\Delta z_{j+1}(\Delta z_j+\Delta z_{j+1})}\right)E_{i,j}^{n}\\&\quad+\frac{\Delta t_{n+1}}{\mu\sigma_{i,j}\Delta z_j(\Delta z_j+\Delta z_{j+1})}E_{i,j-1}^{n}+\frac{\Delta t_{n+1}}{\mu\sigma_{i,j}\Delta z_{j+1}(\Delta z_j+\Delta z_{j+1})}E_{i,j+1}^{n}.\end{aligned}\tag{3.4}$$

For a given index j (j=1,$\cdots$,$J-1$) in the z direction, (3.4) and (3.3) lead to a tridiagonal linear system which could be computed effectively by Thomas' algorithm with a cost of $\mathcal{O}(I)$ [39].

Step 2: Compute E^{n+1} using $E^{n+\frac{1}{2}}$ explicitly in the x direction and implicitly in the z direction.

$$\begin{aligned}&\mu\sigma_{i,j}\frac{E_{i,j}^{n+1}-E_{i,j}^{n+\frac{1}{2}}}{\Delta t_{n+1}/2}=\delta_x^2E_{i,j}^{n+\frac{1}{2}}+\delta_z^2E_{i,j}^{n+1}\\=&\frac{2(E_{i+1,j}^{n+\frac{1}{2}}-E_{i,j}^{n+\frac{1}{2}})}{\Delta x_{i+1}(\Delta x_i+\Delta x_{i+1})}-\frac{2(E_{i,j}^{n+\frac{1}{2}}-E_{i-1,j}^{n+\frac{1}{2}})}{\Delta x_i(\Delta x_i+\Delta x_{i+1})}\\&+\frac{2(E_{i,j+1}^{n+1}-E_{i,j}^{n+1})}{\Delta z_{j+1}(\Delta z_j+\Delta z_{j+1})}-\frac{2(E_{i,j}^{n+1}-E_{i,j-1}^{n+1})}{\Delta z_j(\Delta z_j+\Delta z_{j+1})},\quad i=1,\cdots,I-1,\quad j=1,\cdots,J-1,\end{aligned}\tag{3.5}$$

with the boundary conditions for Γ_2, Γ_3 and Γ_4:

$$E_{i,0}^{n+1}=E_{i,1}^{n+1},\quad E_{0,j}^{n+1}=E_{1,j}^{n+1},\quad E_{I,j}^{n+1}=E_{I-1,j}^{n+1}.\tag{3.6}$$

The numerical scheme for the upper boundary Γ_1 is given by (we will elaborate on this shortly):

$$\frac{3E_{i,J}^{n+1}-4E_{i,J-1}^{n+1}+E_{i,J-2}^{n+1}}{2\Delta z_J}+\frac{1}{\pi}\sum_{k=1}^{I-2}\frac{E_{k+1,J}^{n+1}-E_{k,J}^{n+1}}{x_i-x_{k+\frac{1}{2}}}=0.\tag{3.7}$$

Scheme (3.5) can be rewritten as

$$\begin{aligned}&\left(1+\frac{\Delta t_{n+1}}{\mu\sigma_{i,j}\Delta z_j(\Delta z_j+\Delta z_{j+1})}+\frac{\Delta t_{n+1}}{\mu\sigma_{i,j}\Delta z_{j+1}(\Delta z_j+\Delta z_{j+1})}\right)E_{i,j}^{n+1}\\&\quad-\frac{\Delta t_{n+1}}{\mu\sigma_{i,j}\Delta z_j(\Delta z_j+\Delta z_{j+1})}E_{i,j-1}^{n+1}-\frac{\Delta t_{n+1}}{\mu\sigma_{i,j}\Delta z_{j+1}(\Delta z_j+\Delta z_{j+1})}E_{i,j+1}^{n+1}\end{aligned}$$

$$=\left(1-\frac{\Delta t_{n+1}}{\mu\sigma_{i,j}\Delta x_i(\Delta x_i+\Delta x_{i+1})}-\frac{\Delta t_{n+1}}{\mu\sigma_{i,j}\Delta x_{i+1}(\Delta x_i+\Delta x_{i+1})}\right)E_{i,j}^{n+\frac{1}{2}}$$
$$+\frac{\Delta t_{n+1}}{\mu\sigma_{i,j}\Delta x_i(\Delta x_i+\Delta x_{i+1})}E_{i-1,j}^{n+\frac{1}{2}}+\frac{\Delta t_{n+1}}{\mu\sigma_{i,j}\Delta x_{i+1}(\Delta x_i+\Delta x_{i+1})}E_{i+1,j}^{n+\frac{1}{2}}. \tag{3.8}$$

For a given index i $(i=1,\cdots,I-1)$ in the x direction, a tridiagonal linear system could be constructed by (3.8), (3.6) and (3.7).

For simplicity, we will take homogeneous mesh grids and time steps, that is $\Delta x=\Delta z=h$, $\Delta t=T/N$.

3.0.1 Treatment of the integral boundary condition (2.2)

In the second step of the ADI-FDTD scheme, the electric field at the earth-air interface $E_{i,J}^{n+1}$ $(i=0,\cdots,I)$ must be known in order to make the linear tridiagonal system solvable. This can be achieved by discretizing the boundary condition (2.2) by numerical differential and integral. We approximate the derivative term $\frac{\partial E}{\partial n}$ by:

$$\frac{\partial E^{n+1}}{\partial n}\Big|_{i,J}\doteq\frac{3E_{i,J}^{n+1}-4E_{i,J-1}^{n+1}+E_{i,J-2}^{n+1}}{2h}, \tag{3.9}$$

which is second order accurate. For the integral term, we employ the following discretization:

$$P\int_{-\infty}^{+\infty}\frac{1}{x-x'}\frac{\partial E}{\partial x'}(x',z=b,t^{n+1})dx'\doteq\sum_{k=1}^{I-2}\frac{\delta_x E_{k+\frac{1}{2},J}^{n+1}}{x_i-x_{k+\frac{1}{2}}}h$$
$$=\sum_{k=1}^{I-2}\frac{E_{k+1,J}^{n+1}-E_{k,J}^{n+1}}{x_i-x_{k+\frac{1}{2}}},\quad i=1,\cdots,I-1. \tag{3.10}$$

Substituting (3.9) and (3.10) into (2.2), it leads to (3.7). Note that (3.7) can be rewritten as

$$\frac{3}{2}E_{i,J}^{n+1}-\frac{E_{1,J}^{n+1}}{\pi(i-3/2)}+\frac{E_{I-1,J}^{n+1}}{\pi(i-I+3/2)}+\frac{1}{\pi}\sum_{k=2}^{I-2}\left(\frac{1}{i-k+1/2}-\frac{1}{i-k-1/2}\right)E_{k,J}^{n+1}$$
$$=\frac{4E_{i,J-1}^{n+1}-E_{i,J-2}^{n+1}}{2},\quad i=1,\cdots,I-1. \tag{3.11}$$

From (3.11), it is clear that the values of E^{n+1} at the earth-air interface, i.e. $E_{1:I-1,J}^{n+1}$, can be computed by solving the following linear system:

$$AE_{1:I-1,J}^{n+1}=BE_{1:I-1,J-1}^{n+1}+CE_{1:I-1,J-2}^{n+1}, \tag{3.12}$$

where $B=\mathrm{diag}(2)$, $C=\mathrm{diag}(-\frac{1}{2})$. And the matrix A is given by

$$
\begin{aligned}
&A_{(I-1)\times(I-1)}\\
&=\begin{pmatrix}
\frac{3}{2}+\frac{2}{\pi} & \frac{2}{\pi}(\frac{1}{3}-1) & \frac{2}{\pi}(\frac{1}{5}-\frac{1}{3}) & \cdots & \frac{2}{\pi}(\frac{1}{2I-5}-\frac{1}{2I-7}) & -\frac{2}{\pi}\frac{1}{(2I-5)}\\
-\frac{2}{\pi} & \frac{3}{2}+\frac{4}{\pi} & \frac{2}{\pi}(\frac{1}{3}-1) & \cdots & \frac{2}{\pi}(\frac{1}{2I-7}-\frac{1}{2I-9}) & -\frac{2}{\pi}\frac{1}{(2I-7)}\\
-\frac{2}{\pi}\frac{1}{3} & \frac{2}{\pi}(\frac{1}{3}-1) & \frac{3}{2}+\frac{4}{\pi} & \cdots & \frac{2}{\pi}(\frac{1}{2I-9}-\frac{1}{2I-11}) & -\frac{2}{\pi}\frac{1}{(2I-9)}\\
\vdots & \vdots & \vdots & \cdots & \vdots & \vdots\\
-\frac{2}{\pi}\frac{1}{(2I-7)} & \frac{2}{\pi}(\frac{1}{2I-7}-\frac{1}{2I-9}) & \frac{2}{\pi}(\frac{1}{2I-9}-\frac{1}{2I-11}) & \cdots & \frac{3}{2}+\frac{4}{\pi} & -\frac{2}{\pi}\\
-\frac{2}{\pi}\frac{1}{(2I-5)} & \frac{2}{\pi}(\frac{1}{2I-5}-\frac{1}{2I-7}) & \frac{2}{\pi}(\frac{1}{2I-7}-\frac{1}{2I-9}) & \cdots & \frac{2}{\pi}(\frac{1}{3}-1) & \frac{3}{2}+\frac{2}{\pi}
\end{pmatrix}\\
&=\begin{pmatrix}
\beta(1) & \alpha^T & \beta_1(1)\\
\beta(2:I-2) & A_0 & \beta_1(2:I-2)\\
\beta(I-1) & \alpha_1^T & \beta_1(I-1)
\end{pmatrix},
\end{aligned}
\tag{3.13}
$$

where

$$
\begin{aligned}
&\beta=A(1:I-1,\,1)=\left(\frac{3}{2}+\frac{2}{\pi},\,-\frac{2}{\pi},\,\cdots,\,-\frac{2}{\pi}\frac{1}{(2I-5)}\right)^T,\\
&\beta_1=A(1:I-1,\,I-1)=\left(-\frac{2}{\pi}\frac{1}{(2I-5)},\,-\frac{2}{\pi}\frac{1}{(2I-7)},\,\cdots,\,\frac{3}{2}+\frac{2}{\pi}\right)^T,\\
&\alpha=A(1,\,2:I-2)^T=\left(\frac{2}{\pi}\Big(\frac{1}{3}-1\Big),\,\frac{2}{\pi}\Big(\frac{1}{5}-\frac{1}{3}\Big),\,\cdots,\,\frac{2}{\pi}\Big(\frac{1}{2I-5}-\frac{1}{2I-7}\Big)\right)^T,\\
&\alpha_1=A(I-1,\,2:I-2)^T=\left(\frac{2}{\pi}\Big(\frac{1}{2I-5}-\frac{1}{2I-7}\Big),\,\frac{2}{\pi}\Big(\frac{1}{2I-7}-\frac{1}{2I-9}\Big),\,\cdots,\,\frac{2}{\pi}\Big(\frac{1}{3}-1\Big)\right)^T.
\end{aligned}
\tag{3.14}
$$

It is obvious that A_0 is an $(I-3)\times(I-3)$ symmetric matrix.

However, with the unknowns $E^{n+1}_{1:I-1,J-1}$ and $E^{n+1}_{1:I-1,J-2}$ in (3.12), it is impossible to compute $E^{n+1}_{1:I-1,J}$. To resolve the problem, we could eliminate $E^{n+1}_{1:I-1,J-1}$ and $E^{n+1}_{1:I-1,J-2}$ using (3.5).

First let us express the system (3.5) in a matrix form, for each i from 1 to $I-1$, we have

$$PE^{n+1}_{i,1:J}=F, \tag{3.15}$$

with

$$
P=\begin{pmatrix}
-a & 1+a & 0 & 0 & \cdots & 0 & 0\\
-a & 1+2a & -a & 0 & \cdots & 0 & 0\\
\vdots & \vdots & \vdots & \vdots & & \vdots & \vdots\\
0 & 0 & \cdots & -a & 1+2a & -a & 0\\
0 & 0 & \cdots & 0 & -a & 1+2a & -a
\end{pmatrix}_{(J-1)\times(J)},
\tag{3.16}
$$

where $a=\frac{\Delta t}{2\mu\sigma h^2}$, F represents the RHS of this linear system.

Now, the downward recursion algorithm could be applied to the tridiagonal system (3.15) to eliminate the lower diagonal and render the diagonal elements to be ones (upper triangularization). The last two equations in the system are given by

$$E^{n+1}_{i,J-1}=p^{n+1}_{i,1}E^{n+1}_{i,J}+q^{n+1}_{i,1},\quad E^{n+1}_{i,J-2}=p^{n+1}_{i,2}E^{n+1}_{i,J-1}+q^{n+1}_{i,2}. \tag{3.17}$$

Substituting the first equation of (3.17) into the second one, we obtain

$$E^{n+1}_{i,J-2}=p^{n+1}_{i,1}p^{n+1}_{i,2}E^{n+1}_{i,J}+p^{n+1}_{i,2}q^{n+1}_{i,1}+q^{n+1}_{i,2}. \tag{3.18}$$

Using (3.17) and (3.18), we could replace $E^{n+1}_{1:I-1,J-1}$ and $E^{n+1}_{1:I-1,J-2}$ in (3.12) to complete the linear system with respect to $E^{n+1}_{1:I-1,J}$ and solve it by a linear solver. With the values of $E^{n+1}_{1:I-1,J}$, the second step of the ADI-FDTD scheme can be implemented.

Remark 3.1. The proposed ADI-FDTD scheme is easy and efficient to implement. For the integral boundary condition (2.2), there is only one extra linear system to compute in each iteration besides a sequence of tridiagonal linear systems. However, the extra cost is negligible since there are many fast solvers. In addition, in each substep, the original 2D problem is transformed to a series of 1D problems with tridiagonal linear systems.

4 Stability analysis of ADI-FDTD in L^2 norm

Now, we analyze the stability of the proposed ADI-FDTD scheme for the model (2.1)-(2.4). Firstly, define the following discrete L^2 norms and the corresponding inner product:

$$\begin{aligned}
&||E^n||^2=\sum_{j=1}^{J-1}\sum_{i=1}^{I-1}E^{n^2}_{i,j}h^2,\quad ||\delta_x E^n||^2=\sum_{j=1}^{J-1}\sum_{i=0}^{I-1}(\delta_x E^n_{i+\frac{1}{2},j})^2h^2,\\
&||\delta_z E^n||^2=\sum_{j=0}^{J-1}\sum_{i=1}^{I-1}(\delta_z E^n_{i,j+\frac{1}{2}})^2h^2,\quad ||\delta_x\delta_z E^n||^2=\sum_{j=0}^{J-1}\sum_{i=0}^{I-1}(\delta_x\delta_z E^n_{i+\frac{1}{2},j+\frac{1}{2}})^2h^2,\\
&(U,V)=\sum_{j=1}^{J-1}\sum_{i=1}^{I-1}U_{i,j}V_{i,j}h^2,
\end{aligned} \tag{4.1}$$

and

$$||E^n||^2_{\Gamma_1}=\sum_{i=1}^{I-1}E^{n^2}_{i,J}\frac{h^2}{2},\ ||E^n||^2_{\Gamma_2}=\sum_{j=1}^{J-1}E^{n^2}_{I,j}\frac{h^2}{2},\ ||E^n||^2_{\Gamma_3}=\sum_{i=1}^{I-1}E^{n^2}_{i,0}\frac{h^2}{2},\ ||E^n||^2_{\Gamma_4}=\sum_{j=1}^{J-1}E^{n^2}_{0,j}\frac{h^2}{2}, \tag{4.2}$$

where Γ_1 refers to the earth-air interface, Γ_2, Γ_3 and Γ_4 are the three subsurfaces counterclockwise as shown in Fig. 1.

The discrete L^2 norm of E in the inner domain without boundaries is defined by (4.1), and (4.2) gives the discrete L^2 norm of E on the four boundaries respectively. By estimating the discrete energy of this system, we will analyze the stability of the ADI-FDTD algorithm.

Eliminating the intermediate variables $E^{n+\frac{1}{2}}$ from the schemes (3.2) and (3.5), it is not hard to verify that the ADI scheme is equivalent to the following scheme for all the inner points:

$$\frac{E_{i,j}^{n+1}-E_{i,j}^{n}}{\Delta t}-\frac{1}{2\mu\sigma}(\delta_x^2+\delta_z^2)(E^n+E^{n+1})_{i,j}+\frac{\Delta t}{4\mu^2\sigma^2}\delta_x^2\delta_z^2(E^{n+1}-E^n)_{i,j}=0,$$
$$i=1,\cdots,I-1,\quad j=1,\cdots,J-1. \tag{4.3}$$

Multiplying $(E^n+E^{n+1})_{i,j}$ to both sides of (4.3), computing the inner product and denoting the three items on the left hand side as I_1, I_2 and I_3, respectively, it follows that with the definition in (4.1),

$$\begin{aligned}
I_1&=\left(\frac{E^{n+1}-E^n}{\Delta t},\,(E^n+E^{n+1})\right)=\frac{1}{\Delta t}\left(||E^{n+1}||^2-||E^n||^2\right),\\
I_2&=-\frac{1}{2\mu\sigma}\left((\delta_x^2+\delta_z^2)(E^n+E^{n+1}),\,(E^n+E^{n+1})\right),\\
I_3&=\frac{\Delta t}{4\mu^2\sigma^2}\left(\delta_x^2\delta_z^2(E^{n+1}-E^n),\,(E^n+E^{n+1})\right).
\end{aligned} \tag{4.4}$$

Using the discrete Green formula and imposing the Neumann boundary conditions on the subsurface Γ_2, Γ_3 and Γ_4 (3.6), for the δ_x^2 and δ_z^2 terms in I_2, we deduce respectively, that

$$I_{2_1}=-\frac{1}{2\mu\sigma}\left(\delta_x^2(E^n+E^{n+1}),\,(E^n+E^{n+1})\right)=\frac{1}{2\mu\sigma}||\delta_x(E^n+E^{n+1})||^2, \tag{4.5}$$

$$\begin{aligned}
I_{2_2}&=-\frac{1}{2\mu\sigma}\left(\delta_z^2(E^n+E^{n+1}),\,(E^n+E^{n+1})\right)\\
&=\frac{1}{2\mu\sigma}\left\{||\delta_z(E^n+E^{n+1})||^2-\sum_{i=1}^{I-1}\left[(E^n+E^{n+1})_{i,J}-(E^n+E^{n+1})_{i,J-1}\right]\times(E^n+E^{n+1})_{i,J}\right\}.
\end{aligned} \tag{4.6}$$

In fact, the boundary schemes on subsurfaces $\Gamma_2-\Gamma_4$ (3.6) imply the following relationship:

$$\begin{aligned}
&\delta_z E_{0,j+\frac{1}{2}}^n=\delta_z E_{1,j+\frac{1}{2}}^n,\quad \delta_z E_{I,j+\frac{1}{2}}^n=\delta_z E_{I-1,j+\frac{1}{2}}^n,\quad j=0,\cdots,J-1,\\
&\delta_x E_{i+\frac{1}{2},0}^n=\delta_x E_{i+\frac{1}{2},1}^n,\quad i=0,\cdots,I-1.
\end{aligned} \tag{4.7}$$

By the discrete Green formula and (4.7), for I_3, we derive

$$\begin{aligned}
I_3 &= \frac{\Delta t}{4\mu^2\sigma^2}\sum_{j=1}^{J-1}\sum_{i=1}^{I-1}\delta_x^2\delta_z^2(E^{n+1}-E^n)_{i,j}(E^{n+1}+E^n)_{i,j}h^2 \\
&= \frac{\Delta t}{4\mu^2\sigma^2}\Bigg\{||\delta_x\delta_z E^{n+1}||^2-||\delta_x\delta_z E^n||^2 \\
&\quad -\sum_{i=0}^{I-1}\left[\delta_x(E^{n+1}-E^n)_{i+\frac{1}{2},J}-\delta_x(E^{n+1}-E^n)_{i+\frac{1}{2},J-1}\right]\times\delta_x(E^n+E^{n+1})_{i+\frac{1}{2},J}\Bigg\}. \qquad (4.8)
\end{aligned}$$

The last terms in the RHS of (4.6) and (4.8) need to be dealt with carefully, since they involve the values of E at the earth-air interface.

Firstly, we introduce the following lemma.

Lemma 4.1. *Assume that $E(x,z,t)$ is the exact solution of the IBV problem* (2.1)-(2.4)*, which is of sufficient smoothness, and $E_{i,j}^n$ is the numerical solution of the ADI-FDTD scheme* (3.2)-(3.6)*. Then there exists a constant $\overline{C}$ independent of Δt and h, such that*

$$||E^n||_{\Gamma_1}^2 \le \overline{C}\sum_{i=1}^{I-1}\left(E_{i,J-1}^{n^2}+E_{i,J-2}^{n^2}\right)h^2. \qquad (4.9)$$

Proof. Taking the inner product of $E_{1:I-1,J}$ with both sides of (3.12) at the n-th time level, and considering the left-hand side $E_{1:I-1,J}^{n^T}AE_{1:I-1,J}^n$ (A is of the form (3.13)), we have

$$\begin{aligned}
&E_{1:I-1,J}^{n^T}AE_{1:I-1,J}^n \\
=&E_{2:I-2,J}^{n^T}A_0E_{2:I-2,J}^n+E_{1:I-1,J}^{n^T}\beta E_{1,J}^n+E_{1:I-1,J}^{n^T}\beta_1E_{I-1,J}^n \\
&+\sum_{k=2}^{I-2}E_{1,J}^n\alpha(k-1)E_{k,J}^n+\sum_{k=2}^{I-2}E_{I-1,J}^n\alpha_1(k-1)E_{k,J}^n \\
=&E_{2:I-2,J}^{n^T}A_0E_{2:I-2,J}^n+\beta(1)\left(E_{I-1,J}^{n^2}+E_{1,J}^{n^2}\right)+2\beta(I-1)E_{1,J}^nE_{I-1,J}^n \\
&+\sum_{k=2}^{I-2}\left(\alpha(I-k-1)+\beta(I-k)\right)E_{k,J}^nE_{I-1,J}^n \\
&+\sum_{k=2}^{I-2}\left(\alpha(k-1)+\beta(k)\right)E_{k,J}^nE_{1,J}^n. \qquad (4.10)
\end{aligned}$$

Note that A_0 is a symmetric and strictly diagonal-dominant matrix, thus A_0 is positive-definite and we can estimate its eigenvalues, that is,

$$\left(\frac{3}{2}+\frac{4}{\pi(I-3)}\right)\le\lambda(A_0)\le\left(\frac{3}{2}+\frac{8}{\pi}\right). \qquad (4.11)$$

In addition, by applying the Cauchy-Schwartz inequality, monotonic decreasing and convergence of some series, we conclude that the bound of $||E^n||^2_{\Gamma_1}$ is given by:

$$||E^n||^2_{\Gamma_1}=\sum_{k=1}^{I-1}E^{n^2}_{k,J}\frac{h^2}{2}\leq M_1\sum_{k=1}^{I-1}E^{n^2}_{k,J-1}\frac{h^2}{2}+M_2\sum_{k=1}^{I-1}E^{n^2}_{k,J-2}\frac{h^2}{2}, \tag{4.12}$$

where

$$M_1=1/\left(\frac{3C_1}{2}-C_1^2-\frac{C_1C_2}{4}+\frac{4C_1}{\pi(I-3)}-\frac{50C_0C_1}{9\pi}\right),$$
$$M_2=1/\left(6C_2-4C_1C_2-C_2^2+\frac{16C_2}{\pi(I-3)}-\frac{200C_0C_2}{9\pi}\right),$$

C_1,C_2 are some positive constants independent of Δt and h.

Therefore, it confirms (4.9) with $\overline{C}=\max\{\frac{M_1}{2},\frac{M_2}{2}\}$. □

Remark 4.1. Lemma 4.1 reflects that the energy on the boundaries could be bounded by the inner energy, that is,

$$||E^n||^2_{\Gamma_1}\leq\overline{C}||E^n||^2. \tag{4.13}$$

Using Lemma 4.1, we can treat the last terms in the RHS of I_{2_2} and I_3 to present the following result,

$$\begin{aligned}&||E^{n+1}||^2+\frac{\Delta t^2}{4\mu^2\sigma^2}||\delta_x\delta_zE^{n+1}||^2\\ \leq&||E^n||^2+\frac{\Delta t^2}{4\mu^2\sigma^2}||\delta_x\delta_zE^n||^2+\left(\frac{\Delta tM}{2\mu\sigma h^2}+\frac{\Delta t^2M}{\mu^2\sigma^2h^4}\right)(||E^n||^2+||E^{n+1}||^2),\end{aligned} \tag{4.14}$$

where $M=\max(3M_1+1,3M_2)$.

Summing n for both sides of (4.14), we obtain

$$\begin{aligned}&||E^n||^2+\frac{\Delta t^2}{4\mu^2\sigma^2}||\delta_x\delta_zE^n||^2\\ \leq&||E^0||^2+\frac{\Delta t^2}{4\mu^2\sigma^2}||\delta_x\delta_zE^0||^2+2\Delta t\left(\frac{M}{2\mu\sigma h^2}+\frac{\Delta tM}{\mu^2\sigma^2h^4}\right)\sum_{k=0}^{n}||E^k||^2.\end{aligned} \tag{4.15}$$

By the Gronwall inequality [13], it implies that:

$$\max_{n\leq[T/\Delta t]}||E^n||^2\leq e^{\left(\frac{M}{\mu\sigma h^2}+\frac{2\Delta tM}{\mu^2\sigma^2h^4}\right)T}||E^0||^2. \tag{4.16}$$

In a typical TEM problem, the spatial step h is frequently taken as no less than 10 due to the large scale of the computational domain (10^3-10^4), but the time step Δt is

$\mathcal{O}(10^{-6})$. The total simulation time for receiving the EM response is generally of the 10^{-3} order, thus the exponential term $e^{\left(\frac{M}{\mu\sigma h^2}+\frac{2\Delta t M}{\mu^2\sigma^2 h^4}\right)T}$ could be bounded by some constant. We now derive the stability conclusion of the TEM problem as follows.

Theorem 4.1. *(Stability) Assume that $E(x,z,t)$ is the exact solution of Eqs.* (2.1)-(2.4) *and is of sufficient smoothness. Let $E^n_{i,j}$ be the numerical solution of the ADI scheme* (3.2)-(3.6)*, with the definition of discrete L^2 norm, there exists a positive constant K, such that*

$$\max_{n\leq[T/\Delta t]}||E^n||^2\leq e^{KT}||E^0||^2. \tag{4.17}$$

5 Convergence analysis of ADI-FDTD

We further analyze the convergence of the proposed algorithm by the energy method.

First, the error is defined by,

$$\xi^n_{i,j}=E(x_i,z_j,t^n)-E^n_{i,j},\quad i=0,\cdots,I,\quad j=0,\cdots,J. \tag{5.1}$$

For the truncation error at all interior and boundary grids, we have the following lemma.

Lemma 5.1. *Assume that $E(x,z,t)$ is the exact solution of the IBV problem* (2.1)-(2.4) *and is of sufficient smoothness. Let $E^n_{i,j}$ be the numerical solution of the ADI-FDTD scheme* (3.2)-(3.6)*, it holds that*

$$\begin{aligned}
&\max_{i=1,\cdots,I-1,j=1,\cdots,J-1}\left\{|R^{n+\frac{1}{2}}_{i,j}|\right\}\leq\mathcal{O}(\Delta t^2+h^2),\\
&\max_{j=0,\cdots,J}\left\{|\xi^n_{0,j}|,\,|\xi^n_{I,j}|\right\}\leq\mathcal{O}(\Delta t^2+h^2),\\
&\max_{i=1,\cdots,I-1}\left\{|\xi^n_{i,0}|,\,|\widetilde{R}^n_{i,J}|\right\}\leq\mathcal{O}(\Delta t^2+h^2),
\end{aligned} \tag{5.2}$$

where $R^{n+\frac{1}{2}}_{i,j}$ denotes the truncation error for the interior points, $\xi^n_{I,j}$, $\xi^n_{i,0}$, $\xi^n_{0,j}$ represent the truncation errors on the three subsurfaces $\Gamma_2-\Gamma_4$, respectively and $\widetilde{R}^n_{i,J}$ is the truncation error at the earth-air interface Γ_1.

Proof. For the interior points, from the inner equivalent scheme (4.3), we derive the error equation:

$$\begin{aligned}
\frac{\xi^{n+1}_{i,j}-\xi^n_{i,j}}{\Delta t}-\frac{1}{2\mu\sigma}(\delta_x^2+\delta_z^2)(\xi^n+\xi^{n+1})_{i,j}+\frac{\Delta t}{4\mu^2\sigma^2}\delta_x^2\delta_z^2(\xi^{n+1}-\xi^n)_{i,j}=R^{n+\frac{1}{2}}_{i,j},\\
i=1,\cdots,I-1,\quad j=1,\cdots,J-1.
\end{aligned} \tag{5.3}$$

By Taylor expansion,

$$R_{i,j}^{n+\frac{1}{2}}=\frac{E(x_i,z_j,t^{n+1})-E(x_i,z_j,t^n)}{\Delta t}-\frac{1}{2\mu\sigma}(\delta_x^2+\delta_z^2)\big\{E(x_i,z_j,t^n)$$
$$+E(x_i,z_j,t^{n+1})\big\}+\frac{\Delta t}{4\mu^2\sigma^2}\delta_x^2\delta_z^2\big\{E(x_i,z_j,t^{n+1})-E(x_i,z_j,t^n)\big\}$$
$$=\mathcal{O}(\Delta t^2+h^2),\quad i=1,\cdots,I-1,\ j=1,\cdots,J-1. \tag{5.4}$$

Secondly, in view of the boundary schemes for the subsurfaces (3.6), by Taylor expansion, we have,

$$\xi_{0,j}^n=E(x_0,z_j,t^n)-E_{0,j}^n=\xi_{1,j}^n-\frac{h^2}{2}\frac{\partial^2 E}{\partial x^2}(x_0,z_j,t^n)+\mathcal{O}(h^3),\quad j=0,\cdots,J. \tag{5.5}$$

Similarly,

$$\xi_{I,j}^n=\xi_{I-1,j}^n-\frac{h^2}{2}\frac{\partial^2 E}{\partial x^2}(x_I,z_j,t^n)+\mathcal{O}(h^3),\quad j=0,\cdots,J,$$
$$\xi_{i,0}^n=\xi_{i,1}^n-\frac{h^2}{2}\frac{\partial^2 E}{\partial z^2}(x_i,z_0,t^n)+\mathcal{O}(h^3),\quad i=0,\cdots,I. \tag{5.6}$$

By considering the scheme for the earth-air interface (3.9) and (3.10), we have the corresponding error equation

$$\frac{3\xi_{i,J}^n-4\xi_{i,J-1}^n+\xi_{i,J-2}^n}{2h}+\frac{1}{\pi}\sum_{k=1}^{I-2}\frac{\xi_{k+1,J}^n-\xi_{k,J}^n}{x_i-x_{k+\frac{1}{2}}}=\widetilde{R}_{i,J}^n,\quad i=1,\cdots,I-1. \tag{5.7}$$

Using Taylor expansion and the upward continuation (2.2), we have:

$$\widetilde{R}_{i,J}^n=\frac{3E(x_i,z_J,t^n)-4E(x_i,z_{J-1},t^n)+E(x_i,z_{J-2},t^n)}{2h}+\frac{1}{\pi}\sum_{k=1}^{I-2}\frac{E(x_{k+1},z_J,t^n)-E(x_k,z_J,t^n)}{x_i-x_{k+\frac{1}{2}}}$$
$$=\mathcal{O}(h^2)\ \text{(since the mid-point integral formula is } \mathcal{O}(h^2)). \tag{5.8}$$

The proof is completed. □

To derive the error estimation for the ADI-FDTD scheme in the discrete L^2 norm, multiplying both sides of (5.3) with $(\xi_{i,j}^n+\xi_{i,j}^{n+1})$ and computing the inner product, we obtain

$$Err_1=\left(\frac{\xi^{n+1}-\xi^n}{\Delta t},\,\xi^{n+1}+\xi^n\right)=\frac{1}{\Delta t}\big(||\xi^{n+1}||^2-||\xi^n||^2\big),$$
$$Err_2=\left(-\frac{1}{2\mu\sigma}\big(\delta_x^2+\delta_z^2\big)\big(\xi^n+\xi^{n+1}\big),\,\xi^n+\xi^{n+1}\right)=Err_{2_1}+Err_{2_2},$$
$$Err_3=\left(\frac{\Delta t}{4\mu^2\sigma^2}\delta_x^2\delta_z^2\big(\xi^{n+1}-\xi^n\big),\,\xi^{n+1}+\xi^n\right),$$
$$Err_4=\left(R^{n+\frac{1}{2}},\,\xi^n+\xi^{n+1}\right). \tag{5.9}$$

Since Err_{2_1}, Err_{2_2}, Err_3 and Err_4 are estimated using Lemma 5.1 and similar method as that for the stability analysis, thus we will omit the detailed procedures and present the final conclusion,

$$||\xi^n||^2+\frac{\Delta t^2}{4\mu^2\sigma^2h^2}||\delta_x\delta_z\xi^n||^2\leq||\xi^0||^2+\frac{\Delta t^2}{4\mu^2\sigma^2h^2}||\delta_x\delta_z\xi^0||^2 +\Delta t\left(1+\frac{M_0}{\mu\sigma h^2}+\frac{2\Delta tM_0}{\mu^2\sigma^2h^4}\right)\sum_{k=1}^{n}||\xi^k||^2+\mathcal{O}(\Delta t^4+h^4). \quad (5.10)$$

Notice that $\xi_{i,j}^0=0$, and by the Gronwall lemma, we obtain the following theorem.

Theorem 5.1 (Convergence)**.** *Assume that $E(x,z,t)$ is the exact solution of the IVB problem* (2.2)-(2.4) *and is of sufficient smoothness, let $E_{i,j}^n$ be the numerical solution of the ADI-FDTD scheme* (3.2)-(3.6) *and define error $\xi_{i,j}^n=E(x_i,z_j,t^n)-E_{i,j}^n$, then there exists a positive constant M, such that*

$$\max_{n\leq[T/\Delta t]}||\xi^n||\leq M(\Delta t^2+h^2). \quad (5.11)$$

6 Numerical simulation

To validate the proposed ADI-FDTD scheme for 2D TEM models, we present the computational results for the following test cases. Particular attentions will focus on demonstrating the accuracy and performance advantages of the presented algorithm over the popular FDTD method based on DuFort-Frankel method. Three test cases have been taken as test examples to validate our ADI-FDTD considered in [28].

6.1 Half-space

As a first check of the proposed numerical algorithm, we compute the responses of a homogeneous half-space to the shut-off of a steady current in a double line source at the surface. The test case is chosen because the analytical solution is available for both the electric field at the surface and in the half-space. The initial condition is taken as that reported in [28].

The computational domain is [0, 32000m]×[0, 10000m] and the double line source is set at the centre of the earth-air interface with the negative limb located at x=16250m and the positive limb at x=15750m. The current is I=1A and the electric conductivity of the ground is σ=1/300S/m.

In our simulations, the inhomogeneous grids are adopted along x and z directions with an increasing step size according to the distance from the source, with the smallest step size $\Delta x=\Delta z=h_{min}$=10m for the grids near the source. In terms of the initial condition, we take $t_0=2.0\times10^{-6}$ and the top eight-layer electric field is assigned. The time step Δt used in the computation is listed in Table 1.

Table 1: Time steps in second for the ADI-FDTD and DF schemes.

response time(ms)	Δt for DF	Δt for ADI-FDTD
$(0,0.1)$	1.1793e-7	9.4345e-7
$(0.1,1)$	1.1793e-6	1.8869e-5
>1	2.3586e-6	3.7738e-5

We now compare the performance of the developed ADI-FDTD scheme and that based on DF method [28]. The DF scheme is also unconditionally stable, but the time step Δt could not be taken very large in numerical simulations since oscillatory solutions might occur. Compared with the DF-FDTD method, it is worth to note that more accurate numerical results could be achieved by using the proposed ADI-FDTD algorithm.

Using the time steps listed in Table 1, the solution snapshots are shown in Fig. 2, and the corresponding CPU times are reported in Table 2. Due to the transient of the initial electric fields, at the very beginning (generally before 0.1ms), the time steps must be chosen small enough to describe the responses without distortion. Thus it gives rise to a little longer CPU times for the ADI-FDTD method than the DF scheme at the early time. However, consider that the early time is very short compared with the total computational time, the improvement in accuracy (please refer to Figs. 2 and 3) is more significant. In practical applications, the late time responses are generally required instead of the early time responses. From Table 2, after 3ms, the CPU times for these two algorithms are of the same order.

Table 2: CPU time in second for the ADI-FDTD and DF schemes.

simulation time(ms)	DF	ADI-FDTD
0.007	9	52
0.1	128	265
3	442	482
15	1292	1240

The vertical electromotive force (EMF) at the earth-air interface of the numerical solution and the exact solution are shown in Fig. 2, and they could be obtained by measurement. Figs. 2(a) and 2(b) present the short time response to the switched-off of the current in the double line source, while Figs. 2(c) and 2(d) are the long time responses. The relative L_∞ and L^2 errors defined as follows are also illustrated in Fig. 3 with respect to the response time. It is obvious to see that the ADI-FDTD scheme with large time steps produces more accurate solutions than the DF scheme with relatively small time steps. The advantage of using the presented method is clear especially for computing the late time solution. Fig. 3 confirms that when comparing with the numerical solutions by the DF scheme, an improvement in accuracy of an order of magnitude can be achieved by

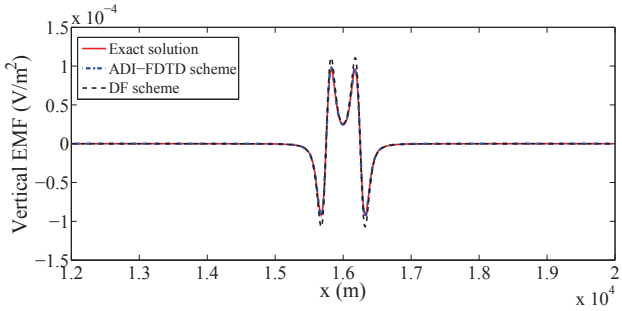

(a) $T=0.007$ms

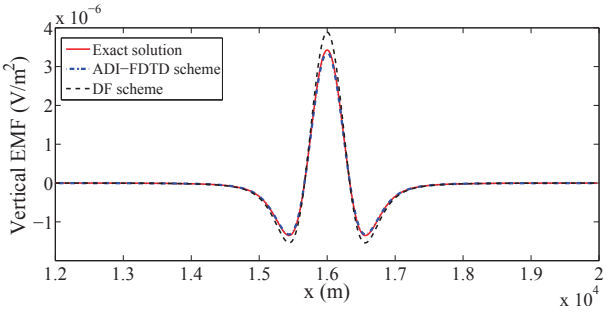

(b) $T=0.1$ms

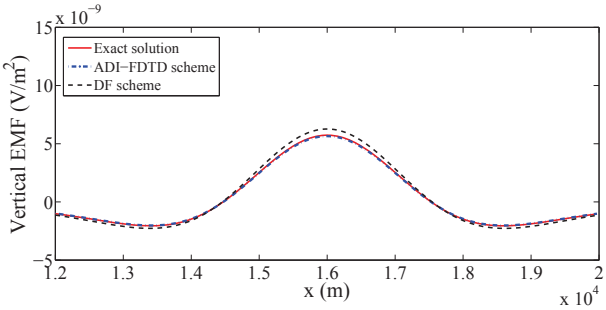

(c) $T=3$ms

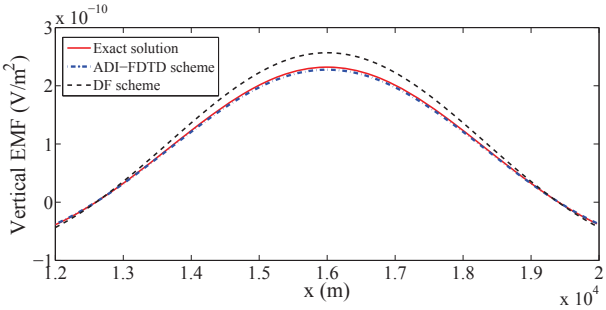

(d) $T=15$ms

Figure 2: Comparison of analytical and numerical solutions computed by the ADI-FDTD and DF schemes for the vertical EMF ($\partial_t B_z$) induced by a double line source on a half-space. Profiles are at (a) 0.007ms, (b) 0.1ms, (c) 3ms, (d) 15ms after the source current was switched off.

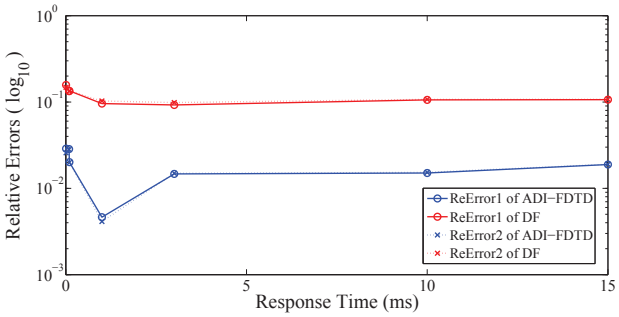

Figure 3: Relative L_∞ and L^2 errors for the ADI-FDTD and DF schemes.

using the ADI-FDTD scheme.

$$ReError1=\frac{||E_{numerical}-E_{exact}||_{L_\infty(\Gamma_1)}}{||E_{exact}||_{L_\infty(\Gamma_1)}},\quad ReError2=\frac{||E_{numerical}-E_{exact}||_{L^2(\Gamma_1)}}{||E_{exact}||_{L^2(\Gamma_1)}}.$$

Fig. 4 gives the contours of the electric field in the whole simulation domain, which

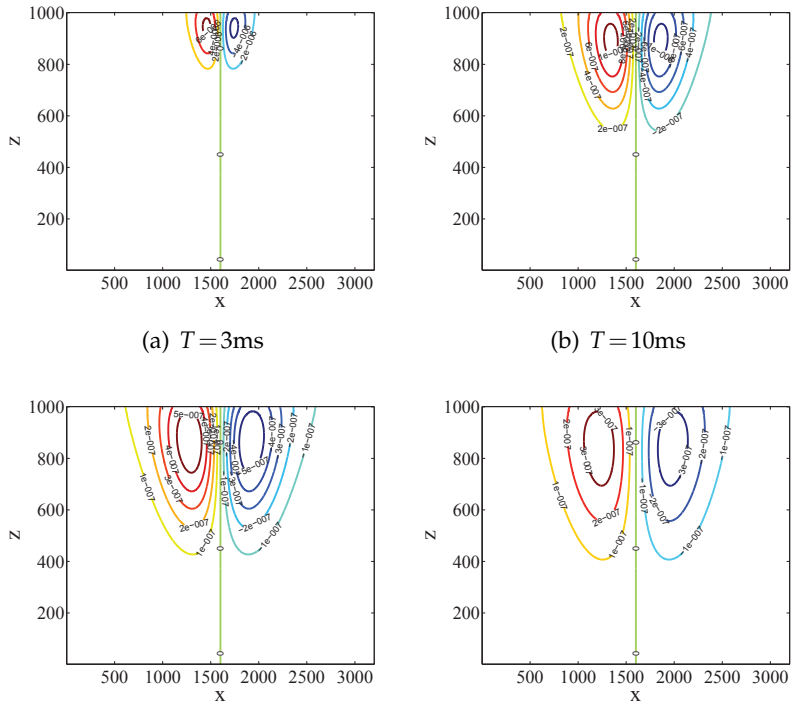

(a) $T=3$ms (b) $T=10$ms

(c) $T=15$ms (d) $T=21$ms

Figure 4: Contours of electric field in a half-space computed by the ADI-FDTD scheme induced by a switched-off 500m wide double line source at the earth-air interface. Profiles are at (a) 3ms, (b) 10ms, (c) 15ms, (d) 21ms after source current was switched off.

illustrates the shape of the induced field propagation. We clearly observe the diffusion of the smoke ring profiles for the electric field as time marching forward.

6.2 Half-space with conductor (large contrast)

The second test case shown in Fig. 5 models a 300Ω-m half-space containing a thin rectangular ore body with the electric conductivity 1000 times more than the surroundings. The thin ore body with the scale of 20m×300m located 300m away from the negative line source to the left along the x direction, thus the distance of the ore body from the center of double line source is about 550m.

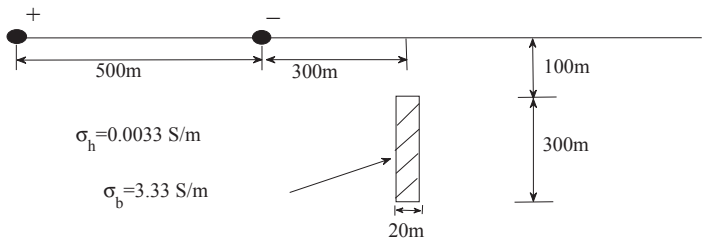

Figure 5: Model geometry for half-space with large-contrast conductor.

In this example, the time steps for the simulation are taken as in Table 3. For the sake of exhibiting the influence of the anomaly elaborately, a small enough Δt is set for the very early time till 0.01ms. Furthermore, after 0.01ms, we adopt much larger time steps compared with DF scheme, which is precisely shown in Table 3 to carry out all the simulations, making the computation efficient and effective. The vertical EMF, horizontal EMF curves and contours of the electric field induced by the switched-off of double line source are reported in Fig. 6, Fig. 7 and Fig. 8, respectively.

Table 3: Time steps in second for ADI-FDTD and DF schemes.

response time (ms)	Δt for DF	Δt for ADI-FDTD
$(0,0.01)$	4.7172e-8	4.7172e-8
$(0.01,0.1)$	1.1793e-7	9.4345e-7
$(0.1,1)$	1.1793e-6	1.8869e-5
>1	2.3586e-6	3.7738e-5

The vertical EMF ($-\partial_t B_z$) profiles using the ADI-FDTD algorithm in Fig. 6 are featured by the crossover from positive to negative values on account of the existence of the thin vertical conductor, and the location of crossover in Fig. 6 is gradually moving to the exact horizontal position of the thin anomaly. In addition, the peak of the horizontal EMF ($-\partial_t B_x$) using the ADI-FDTD algorithm displayed in Fig. 7 could also serve to examine the horizontal position of the thin body approximately.

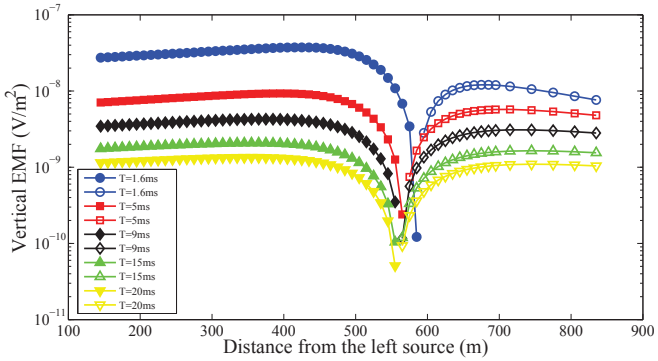

Figure 6: Profiles of the vertical EMF ($\partial_t B_z$) by the ADI-FDTD scheme for the half-space conductor with a 1000:1 contrast. The negative line source is on the right. Open marks indicate negative values and dark marks represent positive ones.

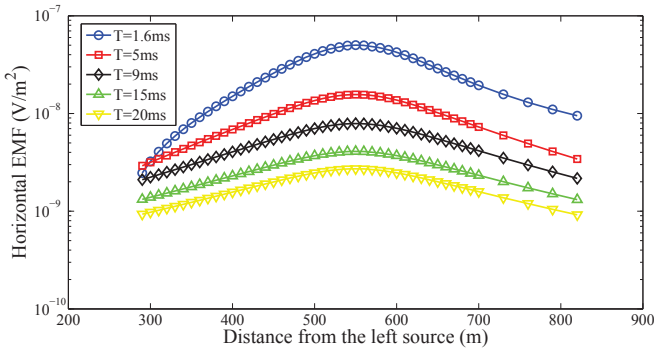

Figure 7: Profiles of the horizontal EMF ($\partial_t B_x$) by the ADI-FDTD scheme for the half-space conductor with a 1000:1 contrast. The negative line source is on the right. Open marks indicate negative values.

Fig. 8 compares the contours of the electric fields for this large contrast model using ADI-FDTD scheme(on the left) as well as DF scheme(on the right) and the snapshots presented cover a wide range of time from the very early time 0.006ms to the late time 20ms. It is clear to see that the two sets of results are generally consistent with each other except for some subtle distinction. Results by the ADI-FDTD method capture the responses well for both early times and late times.

To illustrate the characters of the electric field around the thin conductor and double line source, only the central and uniform region of the numerical grid are shown. The crossover on the left of the first four subfigures makes clear the position of the source center, while the crossover on the right highlights the main domain containing the thin conductor. The following subfigures reflect that when the diffusion of electric field encounters the thin anomaly, they are distorted and perform by the interaction with this conductor. The snapshot taken at 3.7ms displays a fully developed target response and the further evolution of the electric field involves its gradual equalization and decay within the conductor.

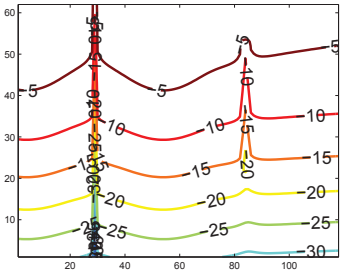

(a) ADI, $T=0.006$ms

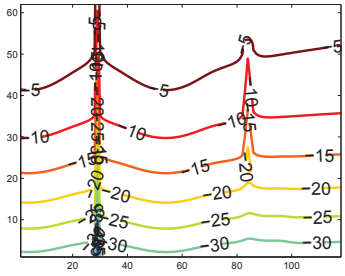

(b) DF, $T=0.006$ms

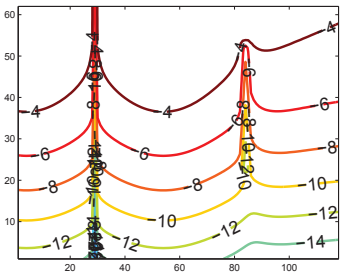

(c) ADI, $T=0.015$ms

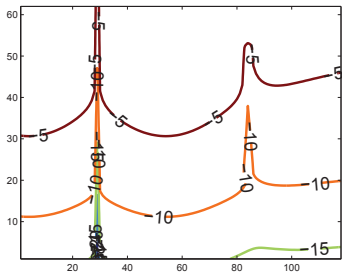

(d) DF, $T=0.015$ms

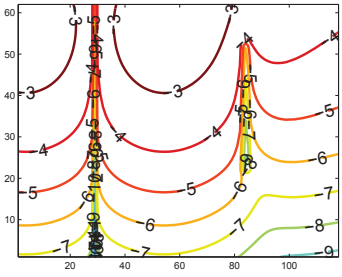

(e) ADI, $T=0.036$ms

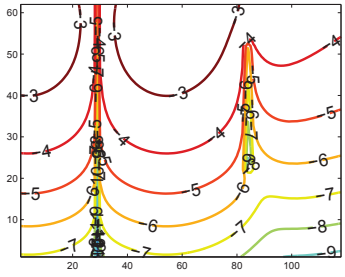

(f) DF, $T=0.036$ms

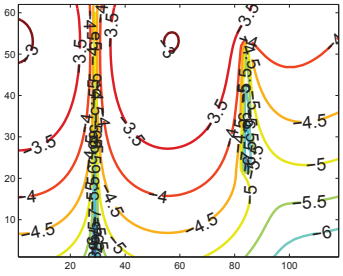

(g) ADI, $T=0.08$ms

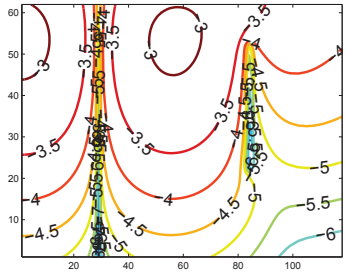

(h) DF, $T=0.08$ms

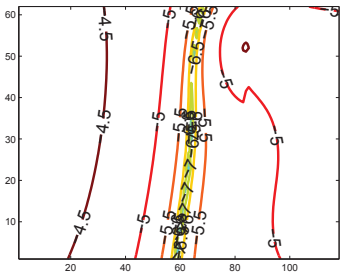

(i) ADI, $T=0.6$ms

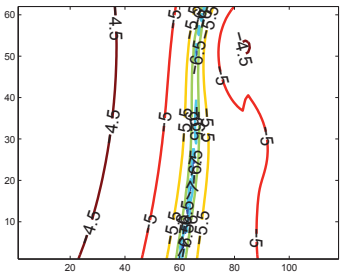

(j) DF, $T=0.6$ms

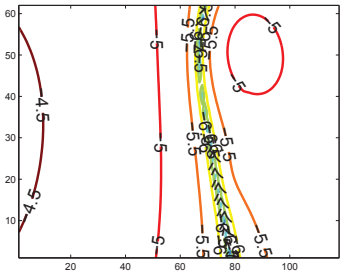

(k) ADI, $T=1.0$ms

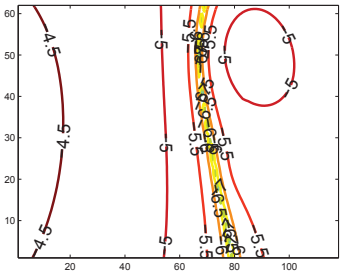

(l) DF, $T=1.0$ms

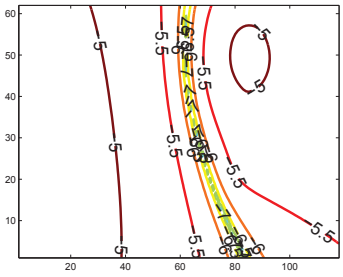

(m) ADI, $T=1.6$ms

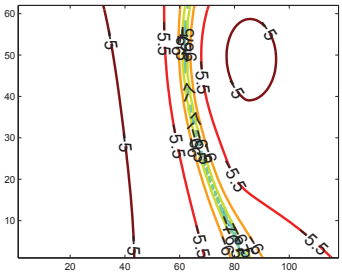

(n) DF, $T=1.6$ms

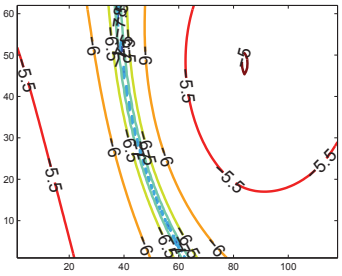

(o) ADI, $T=3.7$ms

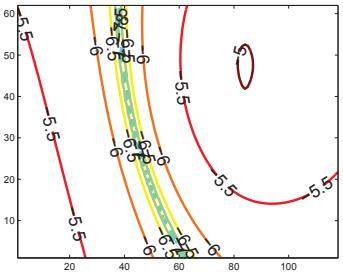

(p) DF, $T=3.7$ms

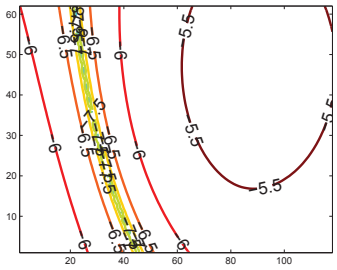

(q) ADI, $T=5$ms

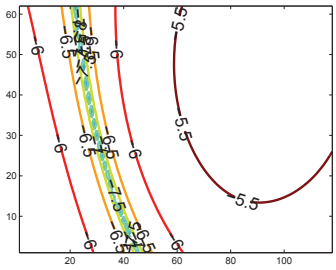

(r) DF, $T=5$ms

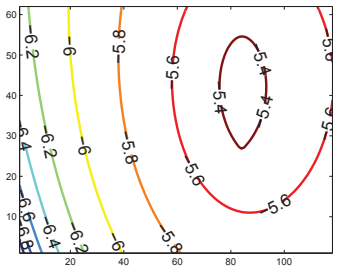

(s) ADI, $T=9$ms

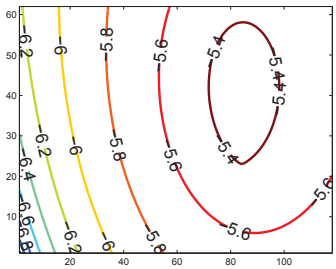

(t) DF, $T=9$ms

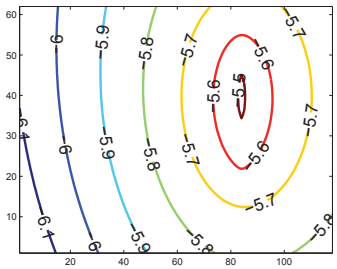

(u) ADI, $T=15$ms

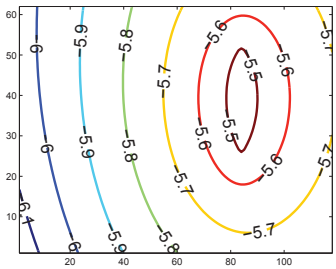

(v) DF, $T=15$ms

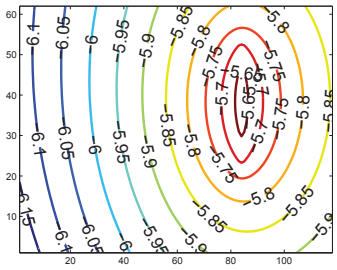

(w) ADI, $T=20$ms

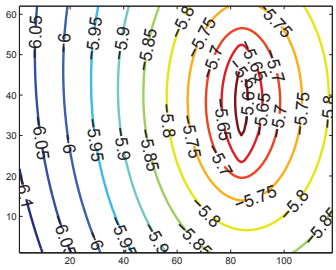

(x) DF, $T=20$ms

Figure 8: Contours of electric field(the values are the logarithm of E) computed by the ADI-FDTD scheme(on the left) and the DF scheme(on the right) for the half-space with the conductor of 1000:1, induced by a switched-off 500m wide double line source at the earth-air interface.

6.3 Half-space with conductor (small contrast)

We now consider a small contrast(100:1) version of the second model as the last example illustrated in Fig. 9. The parameters for this simulation are set the same as those in the large contrast case, except that the half-space resistivity is 100Ω-m, while the body resistivity is 1Ω-m.

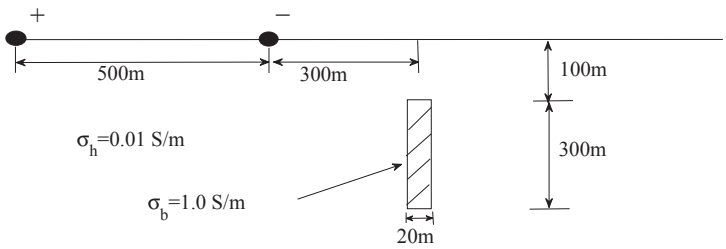

Figure 9: Model geometry for overburden and half-space with small-contrast conductor.

From the vertical EMF presented in Fig. 10, it is clear that even though the crossover appears at nearly the exact target position at 1 ms, it moves to the right and away from the target with time advancing. This may be attributed to the currents in the half-space, whose contribution covers some of the effect from the currents flowing in the ore body.

On the other hand, the horizontal EMF profiles shown in Fig. 11 obviously illustrate the location of the anomaly by their peaks. Generally, in contrast to the crossover point of the vertical EMF, the peak in the horizontal EMF is always directly above the target in the millisecond time range and thus giving a better indication of the conductor location. We also report the snapshots by the ADI-FDTD and DF schemes in Fig. 12 to reveal some details of the development of the electric field in early time and later the interaction between the smoke ring and the conductor, and their results are in good agreement.

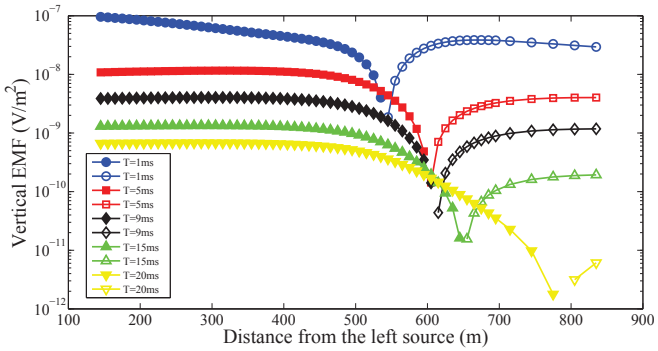

Figure 10: Profiles of the vertical EMF ($\partial_t B_z$) by the ADI-FDTD scheme for the half-space with small contrast conductor model. The negative line source is on the right. Open marks indicate negative values and dark marks represent positive ones.

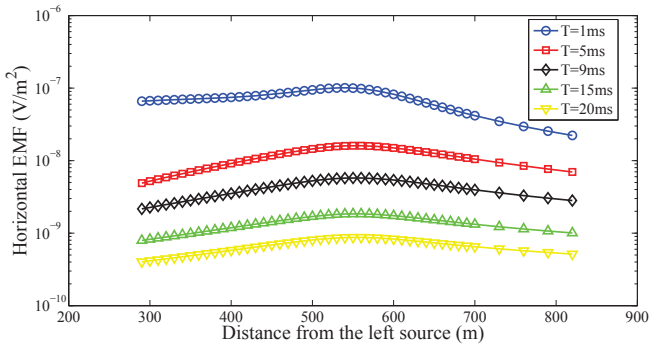

Figure 11: Profiles of the horizontal EMF ($\partial_t B_x$) by the ADI-FDTD scheme for the half-space with small contrast conductor model. The negative line source is on the right. Open marks indicate negative values.

7 Conclusion

We present an efficient and accurate ADI-FDTD algorithm to simulate EM diffusion phenomenon in 2D earth excited by the electric line sources. Comparisons with the analytical and DuFort-Frankel solutions confirm the accuracy and efficiency of the proposed algorithm. The ADI technique is applied such that the resultant tri-diagonal system can be effectively computed by the Thomas algorithm. To ensure an accurate representation for the earth-air interface, an integral formulation is imposed at the interface boundary. A novel numerical discretization scheme for the integral equation is presented and it is incorporated to the ADI scheme implicitly. With the numerical implementation for the integral boundary condition, the stability and convergence analysis for the ADI-FDTD scheme are reported. Numerical simulations clearly demonstrate that the proposed ADI-FDTD scheme produces more accurate computed solutions than those resulted by the DuFort-Frankel scheme both in the early time and late time computation.

It is worth to investigate further applications and improvements of the proposed ADI-FDTD algorithm. For example, consider using the secondary field instead of total field in the model. Secondary field is defined as the difference between the total field and the field of a background model, and they vary more slowly than the total field in both time and space. The application of an absorbing boundary condition including a perfectly matched layer (PML) for the underground interface is also an interesting topic. Finally, it is important to extend the present approach for 2.5D and 3D problems.

Acknowledgments

We would like to thank Professor Tang Tao and the referees for the helpful comments and suggestion. The research was supported in part by the Natural Sciences and Engineering Research Council of Canada. Wanshan Li was supported by the China Scholarship Council for her visit to the University of Alberta, and Dong Liang would like to acknowledge the partial support by the Natural Science Foundation of China under grant 11271232.

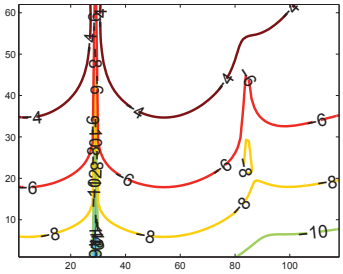

(a) ADI, $T=0.08$ms

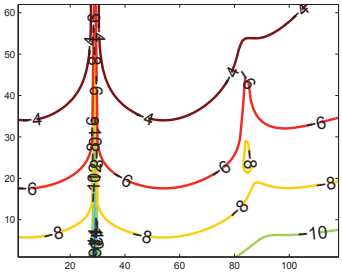

(b) DF, $T=0.08$ms

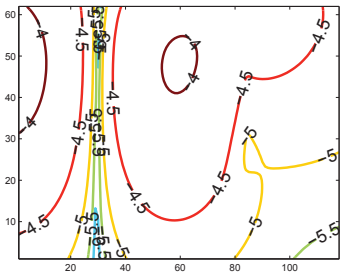

(c) ADI, $T=0.5$ms

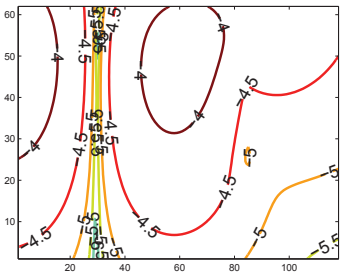

(d) DF, $T=0.5$ms

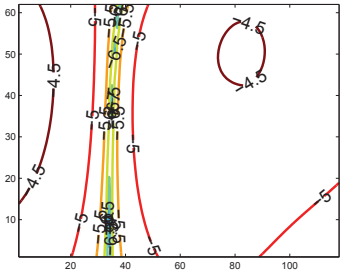

(e) ADI, $T=1$ms

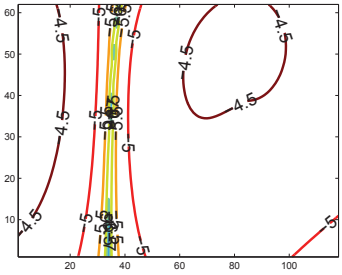

(f) DF, $T=1$ms

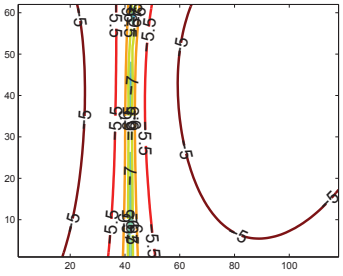

(g) ADI, $T=1.6$ms

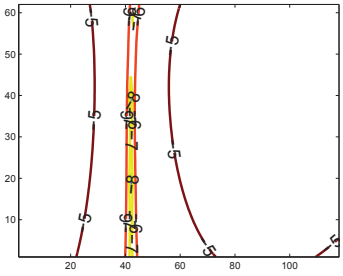

(h) DF, $T=1.6$ms

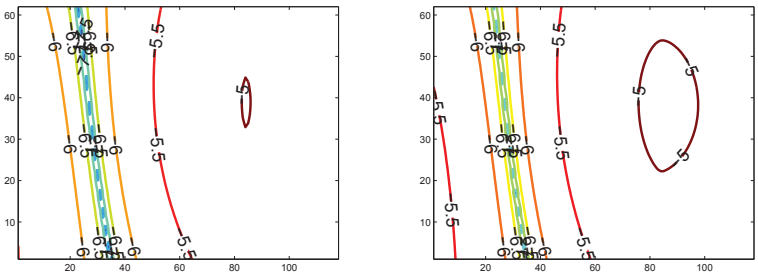

(i) ADI, $T=5$ms (j) DF, $T=5$ms

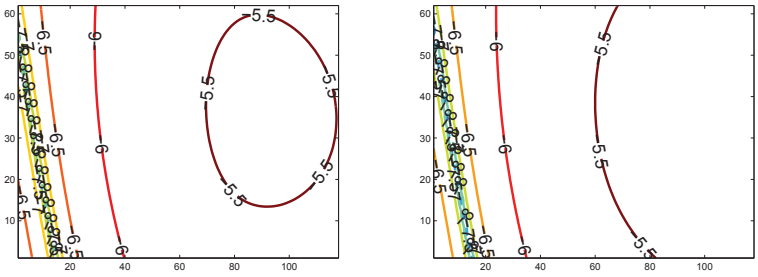

(k) ADI, $T=9$ms (l) DF, $T=9$ms

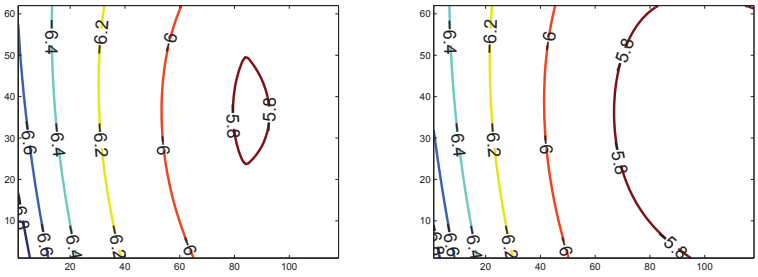

(m) ADI, $T=15$ms (n) DF, $T=15$ms

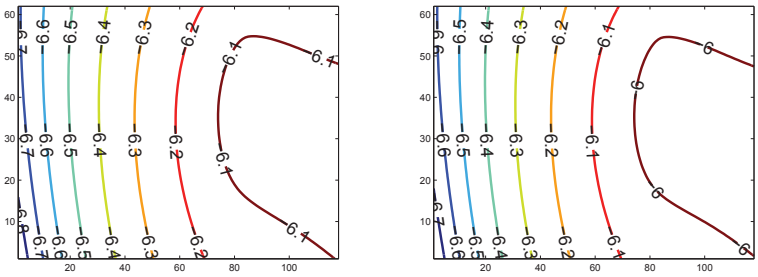

(o) ADI, $T=20$ms (p) DF, $T=20$ms

Figure 12: Contours of electric field(the values are the logarithm of E) computed by the ADI-FDTD scheme(on the left) and the DF scheme(on the right) for the half-space with small contrast conductor model, induced by a switched-off 500m wide double line source at the earth-air interface.

References

[1] J. I. Adhidjaja, G. W. Hohmann and M. L. Oristaglio, Two-dimensional transient electromagnetic responses, Geophysics, 50 (1985), 2849-2861.

[2] W. Chen, X. Li and D. Liang, Symmetric energy-conserved splitting FDTD scheme for the Maxwell's equations, Comm. Comput. Phys., 6 (2009), 804-825.

[3] Y. Chung, J.-S. Son, T. J. Lee, H. J. Kim and C. Shin, Three-dimensional modelling of controlled-source electromagnetic surveys using an edge finite-element method with a direct solver, Geophys. Prospect., 62 (2014), 1468-1483.

[4] M. Commer and G. Newman, A parallel finite-difference approach for 3D transient electromagnetic modeling with galvanic sources, Geophysics, 69 (2004), 1192-1202.

[5] S. Constable and C. J. Weiss, Mapping thin resistors and hydrocarbons with marine EM methods: Insights from 1D modeling, Geophysics, 71 (2006), G43-G51.

[6] N. V. da Silva, J. V. Morgan, L. MacGregor and M. Warner, A finite element multifrontal method for 3D CSEM modeling in the frequency domain, Geophysics, 77 (2012), E101-E115.

[7] M. Everett and R. Edwards, Transient marine electromagnetics: the 2.5-D forward problem, Geophys. J. Int., 113 (1993), 545-561.

[8] R. W. Freund and N. M. Nachtigal, An implementation of the QMR method based on coupled two-term recurrences, SIAM J. Sci. Comput., 15 (1994), 313-337.

[9] L. Gao and D. Liang, New energy-conserved identities and super-convergence of the symmetric EC-S-FDTD scheme for Maxwell's equations in 2D, Comm. Comput. Phys., 11 (2012), 1673-1696.

[10] Y. Goldman, C. Hubans, S. Nicoletis and S. Spitz, A finite-element solution for the transient electromagnetic response of an arbitrary two-dimensional resistivity distribution, Geophysics, 51 (1986), 1450-1461.

[11] A. Grayver, R. Streich and O. Ritter, Three-dimensional parallel distributed inversion of CSEM data using a direct forward solver, Geophys. J. Int., 193 (2013), 1432-1446.

[12] A. V. Grayver and M. Bürg, Robust and scalable 3-D geo-electromagnetic modelling approach using the finite element method, Geophys. J. Int., 198 (2014), 110-125.

[13] T. H. Gronwall, Note on the derivatives with respect to a parameter of the solutions of a system of differential equations, Ann. Math., 20 (1919), 292-296.

[14] E. Haber and U. M. Ascher, Fast finite volume simulation of 3D electromagnetic problems with highly discontinuous coefficients, SIAM J. Sci. Comput., 22 (2001), 1943-1961.

[15] E. Haber and C. Schwarzbach, Parallel inversion of large-scale airborne time-domain electromagnetic data with multiple octree meshes, Inverse Prob., 30 (2014), 055011.

[16] J. Huang and A. Wood, Analysis and numerical solution of transient electromagnetic scattering from overfilled cavities, Comm. Comput. Phys., 1 (2006), 1043-1055.

[17] J. Huang, A. W. Wood and M. J. Havrilla, A hybrid finite element-Laplace transform method for the analysis of transient electromagnetic scattering by an over-filled cavity in the ground plane, Comm. Comput. Phys., 5 (2009), 126-141.

[18] X. Jiang, L. Zhang and W. Zheng, Adaptive hp-finite element computations for time-harmonic Maxwells equations, Comm. Comput. Phys., 13 (2013), 559-582.

[19] Jr. Jim, Douglas, On the numerical integration $\frac{\partial^2 u}{\partial x^2}+\frac{\partial^2 u}{\partial y^2}=\frac{\partial u}{\partial t}$ by implicit methods, J. Soc. Ind. Appl. Math., 3 (1955), 42-65.

[20] K. Key and J. Ovall, A parallel goal-oriented adaptive finite element method for 2.5-D electromagnetic modelling, Geophys. J. Int., 186 (2011), 137-154.

[21] J. Koldan, V. Puzyrev, J. de la Puente, G. Houzeaux and J. M. Cela, Algebraic multigrid pre-

conditioning within parallel finite-element solvers for 3-D electromagnetic modelling problems in geophysics, Geophys. J. Int., 197 (2014), 1442-1458.
[22] J. T. Kuo and D.-h. Cho, Transient time-domain electromagnetics, Geophysics, 45 (1980), 271-291.
[23] K. H. Lee, Electromagnetic scattering by two-dimensional inhomogeneity due to an oscillating magnetic dipole, California Univ., Berkeley (USA), 1978.
[24] M. Leppin, Electromagnetic modeling of 3-D sources over 2-D inhomogeneities in the time domain, Geophysics, 57 (1992), 994-1003.
[25] F. A. Maaø, Fast finite-difference time-domain modeling for marine-subsurface electromagnetic problems, Geophysics, 72 (2007), A19-A23.
[26] S. Mukherjee and M. E. Everett, 3D controlled-source electromagnetic edge-based finite element modeling of conductive and permeable heterogeneities, Geophysics, 76 (2011), F215-F226.
[27] T. Namiki, A new FDTD algorithm based on alternating-direction implicit method, IEEE Trans. Microwave Theory Tech., 47 (1999), 2003-2007.
[28] M. L. Oristaglio and G. W. Hohmann, Diffusion of electromagnetic fields into a two-dimensional earth: A finite-difference approach, Geophysics, 49 (1984), 870-894.
[29] D. W. Peaceman and H. H. Rachford Jr., The numerical solution of parabolic and elliptic differential equations, J. Soc. Ind. Appl. Math., 3 (1955), 28-41.
[30] V. Puzyrev, J. Koldan, J. de la Puente, G. Houzeaux, M. Vázquez and J. M. Cela, A parallel finite-element method for three-dimensional controlled-source electromagnetic forward modelling, Geophys. J. Int., 193 (2013), 678-693.
[31] Z. Ren, T. Kalscheuer, S. Greenhalgh and H. Maurer, A goal-oriented adaptive finite-element approach for plane wave 3-D electromagnetic modelling, Geophys. J. Int., 194 (2013), 700-718.
[32] C. Schwarzbach and E. Haber, Finite element based inversion for time-harmonic electromagnetic problems, Geophys. J. Int., 193 (2013), 615-634.
[33] W. H. T. Sheu, L. Y. Liang and J.-H. Li, Development of an explicit symplectic scheme that optimizes the dispersion-relation equation for the Maxwell's equations, Comm. Comput. Phys., 13 (2013), 1107-1133.
[34] M. Sommer, S. Hölz, M. Moorkamp, A. Swidinsky, B. Heincke, C. Scholl and M. Jegen, GPU parallelization of a three dimensional marine CSEM code, Comput. Geosci., 58 (2013), 91-99.
[35] R. Streich, 3D finite-difference frequency-domain modeling of controlled-source electromagnetic data: Direct solution and optimization for high accuracy, Geophysics, 74 (2009), F95-F105.
[36] R. Streich, M. Becken and O. Ritter, 2.5D controlled-source EM modeling with general 3D source geometries, Geophysics, 76 (2011), F387-F393.
[37] Y. Sun and F. Tao, Symplectic and multisymplectic numerical methods for Maxwell's equations, J. Comput. Phys., 230 (2011), 2076-2094.
[38] A. Taflove, Application of the finite-difference time-domain method to sinusoidal steady-state electromagnetic-penetration problems, IEEE Trans. Electromagn. Compat., 22 (1980), 191-202.
[39] L. Thomas, Elliptic problems in linear difference equations over a network, Technique report, Watson Scientific Computing Laboratory, Columbia University, New York, 1949.
[40] E. S. Um, M. Commer and G. A. Newman, Efficient pre-conditioned iterative solution strategies for the electromagnetic diffusion in the earth: finite-element frequency-domain approach, Geophys. J. Int, 193 (2013), 1460-1473.

[41] E. S. Um, J. M. Harris and D. L. Alumbaugh, 3D time-domain simulation of electromagnetic diffusion phenomena: A finite-element electric-field approach, Geophysics, 75 (2010), F115-F126.
[42] T. Wang and G. W. Hohmann, A finite-difference, time-domain solution for three-dimensional electromagnetic modeling, Geophysics, 58 (1993), 797-809.
[43] Z. Xie, B. Wang and Z. Zhang, Space-time discontinuous Galerkin method for Maxwell's equations, Comm. Comput. Phys., 14 (2013), 916-939.
[44] K. S. Yee et al., Numerical solution of initial boundary value problems involving Maxwells equations in isotropic media, IEEE Trans. Antennas Propag, 14 (1966), 302-307.
[45] M. Zaslavsky, V. Druskin, S. Davydycheva, L. Knizhnerman, A. Abubakar and T. Habashy, Hybrid finite-difference integral equation solver for 3D frequency domain anisotropic electromagnetic problems, Geophysics, 76 (2011), F123-F137.